JACS
JOURNAL OF THE AMERICAN CHEMICAL SOCIETY
pubs.acs.org/JACS
Article

σ-Aromatic Ge−Sn Bridges in a Triply-Bonded Bare Cluster Dimer with a Long-Lived Triplet State

Ya-Shan Huang,[⊥] Ziqi Deng,[⊥] Wen-Juan Tian, Hui-Qing Sun, Alvaro Muñoz-Castro, Teng-Teng Chen,* and Zhong-Ming Sun*

Cite This: J. Am. Chem. Soc. 2025, 147, 45723−45730

ABSTRACT: Constructing extended cluster aggregates requires a deeper understanding of strategies for connecting structural motifs. Herein, we report the synthesis and structural elucidation of the triply bonded dimeric cluster $[(Rh@Sn_8)_2Ge_2]^{4-}$ (**1a**), which features a delocalized bonding framework arising from the connection of two spherical aromatic $[Rh@Sn_8]$ units via two unique 6σ-aromatic $[GeSn_4]$ bridges. The resulting framework simultaneously exhibits global aromaticity and multiple localized aromatic fragments, highlighting a rational route toward controlled cluster growth and offering new synthetic avenues for cluster-based bulk materials. Moreover, femtosecond-to-nanosecond transient absorption spectroscopy revealed an exceptionally long-lived triplet excited state (τ_{av} = 178 μs) for $[(Rh@Sn_8)_2Ge_2]^{4-}$, significantly longer than those reported for metal nanoclusters in the condensed phase. This finding supplements the limited excited-state features of bare metal nanoclusters and provides a new strategy for achieving prolonged excited-state lifetimes in cluster systems.

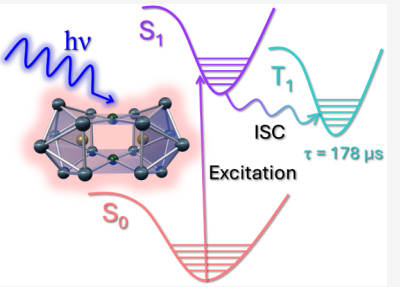

INTRODUCTION

As an intermediate state between atoms or molecules and bulk materials, nanoclusters occupy a unique position in matter's hierarchy, offering exceptional opportunities for the rational design of functional materials. Understanding how their structural units assemble and connect is therefore essential for the development of cluster-based materials with tailored properties.[1] Among potential building motifs, aromatic inorganic units, particularly those with spherical aromaticity, have emerged as versatile precursors for constructing larger cluster aggregates.[2−11] For instance, the clusters $[Ge_{24}]^{4-}$ and $[Sn_{36}]^{8-}$[10,11] are generated via oxidative coupling of spherically aromatic $[Ge_9]^{4-}$ and $[Sn_9]^{4-}$ units, respectively.

Beyond spherical aromatic clusters, planar aromatic species have also attracted attention as promising motifs.[12,13] Their electronic properties can be modulated by partial heteroatom substitution within the aromatic framework, yielding hybrid organic/inorganic benzene analogues.[14,15] In contrast, the synthesis of purely inorganic aromatic compounds, particularly those composed solely of *p*-block elements, is relatively difficult.[16−21] Compared with homonuclear systems, the intrinsic electronegativity differences between heteroatoms often disrupt delocalized bonding, thereby limiting the extent of aromatic stabilization.[22] Previous efforts have yielded several inorganic heteroatomic compounds containing lighter elements (B, N, O, Al, Si, P),[14−16] most of which exhibit planar π-aromatic character.[23−29] Only a few Ge-containing systems have been reported to display combined σ-, π-, and nonbonding electron delocalization,[30−32] yet the realization of well-defined σ-aromatic planes remains a formidable synthetic and conceptual challenge.

In addition to ground-state structural and electronic features, the excited-state properties of inorganic clusters have begun to draw attention, although studies on all-metal clusters remain scarce. Pure clusters composed exclusively of main-group elements or coinage metals typically exhibit extremely short excited-state lifetimes, as nonradiative decay dominates due to their low density of states.[33] Introducing heteroatomic mixing within metal nanoclusters can fundamentally alter their electronic structures, potentially stabilizing excited states and prolonging excited-state lifetimes. Such systems provide ideal models for probing intrinsic photophysical behavior in all-metal frameworks.

In this work, we report the successful synthesis of the $[(Rh@Sn_8)_2Ge_2]^{4-}$ cluster, which features the first σ-aromatic heteroatomic plane composed entirely of *p*-block elements. Such a 6σ-aromatic structure is exceptionally rare. The two $[GeSn_4]$ planes act as bridges connecting two spherical aromatic $[Rh@Sn_8]$ units, resulting in a globally aromatic triply bonded dimer. Furthermore, transient absorption (TA) spectroscopy combined with theoretical calculations[34−37] reveals the ultrafast photophysical properties and identifies a

Received: October 13, 2025
Revised: November 23, 2025
Accepted: November 25, 2025
Published: December 1, 2025

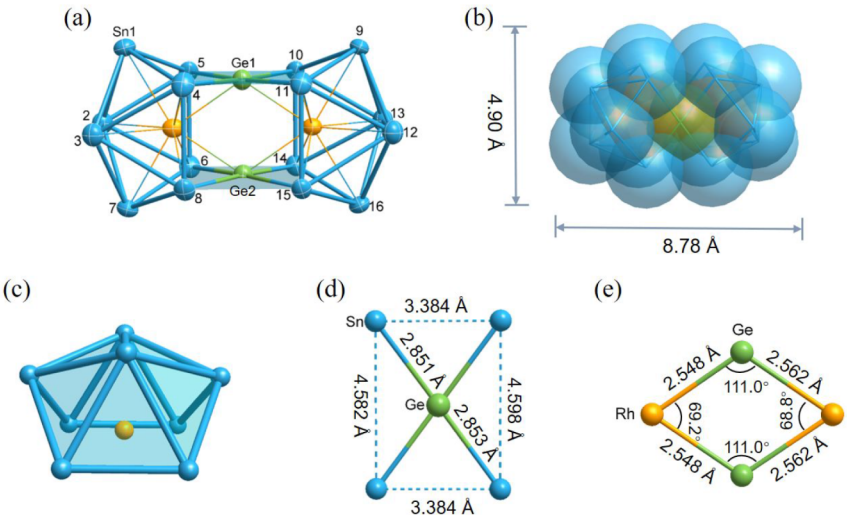

Figure 1. (a) Ellipsoid plot (50% level) of the crystal structure of the cluster $[(Rh@Sn_8)_2Ge_2]^{4-}$; (b) space-filling representation of the cluster $[(Rh@Sn_8)_2Ge_2]^{4-}$; (c) view of the $[Rh@Sn_8]$ cage; (d) the square-planar $[GeSn_4]$ unit; and (e) rhombus-like $[Rh_2Ge_2]$ unit.

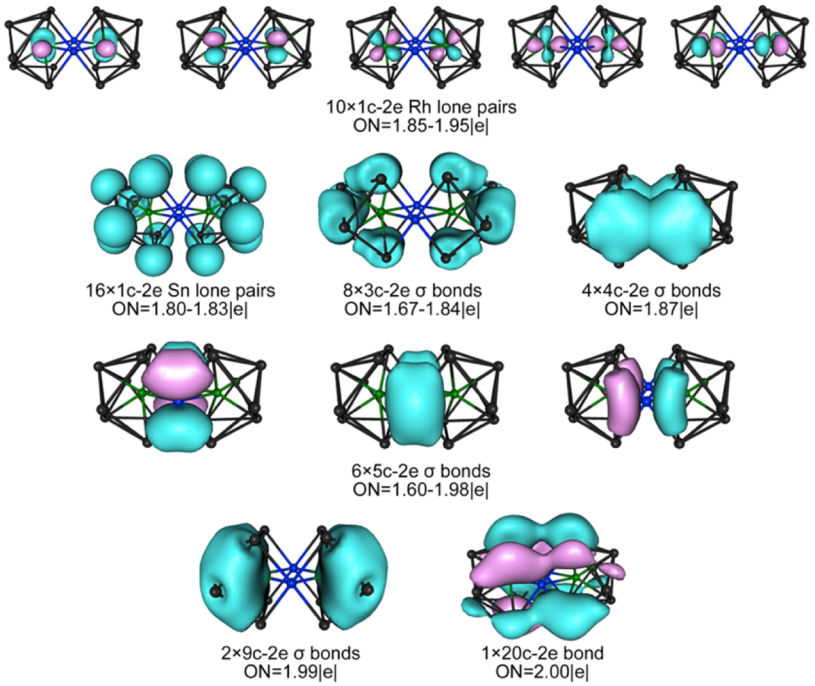

Figure 2. Bonding pattern for cluster **1a** as revealed from the adaptive natural density partitioning (AdNDP) analysis with occupation numbers (ONs) indicated.

remarkably long-lived triplet state (τ = 178 μs) for $[(Rh@Sn_8)_2Ge_2]^{4-}$ in DMF solution. These findings not only demonstrate a new structural paradigm for all-metal nanoclusters but also address a critical gap in understanding their excited-state dynamics, thereby opening new avenues for the design of photoactive cluster-based materials.

RESULTS AND DISCUSSION

Black prism-like crystals of the compound $[K(2.2.2\text{–crypt})]_4[(Rh@Sn_8)_2Ge_2]$ (**1**) was synthesized by reacting $K_4Ge_{4.5}Sn_{4.5}$ with $Rh(PPh_3)_2Cp$ in the presence of 2.2.2-crypt in ethylenediamine (en) solution (Figure S1). The resulting Rh–Ge–Sn ternary species represents one of the few known compounds containing mixed Ge/Sn components.[38−41] This rarity is attributable to the nature of the precursor $K_4Ge_{4.5}Sn_{4.5}$, which exists as $[Ge_{9-x}Sn_x]^{4-}$ in solution.[38] These anions feature uneven charge distributions, high reactivity, and pronounced sensitivity to reaction conditions, thereby hindering the synthesis of novel assembly clusters.[38]

Single-crystal X-ray diffraction revealed that the cluster anion **1a** is disordered at six Sn sites within one of the $[Rh@Sn_8]$ units, resulting in a major component (90%) and a minor component (10%, Figures S2 and S3, Table S1). As both components share nearly identical structural geometries, the discussion below focuses on the major component.

Electrospray-ionization mass spectrometry (ESI-MS) results of crystals of compound **1** dissolved in *N*,*N*-dimethylformamide (DMF) displayed three primary peaks corresponding to the parent species: $\{[Rh_2Sn_{16}Ge_2]\}^{2-}$, $\{[Rh_2Sn_{16}Ge_2]\}^{-}$, and $\{[K(2.2.2\text{-crypt})][Rh_2Sn_{16}Ge_2]\}^{-}$ (Figures S4–S7). Additional

https://doi.org/10.1021/jacs.5c18030
J. Am. Chem. Soc. 2025, 147, 45723−45730

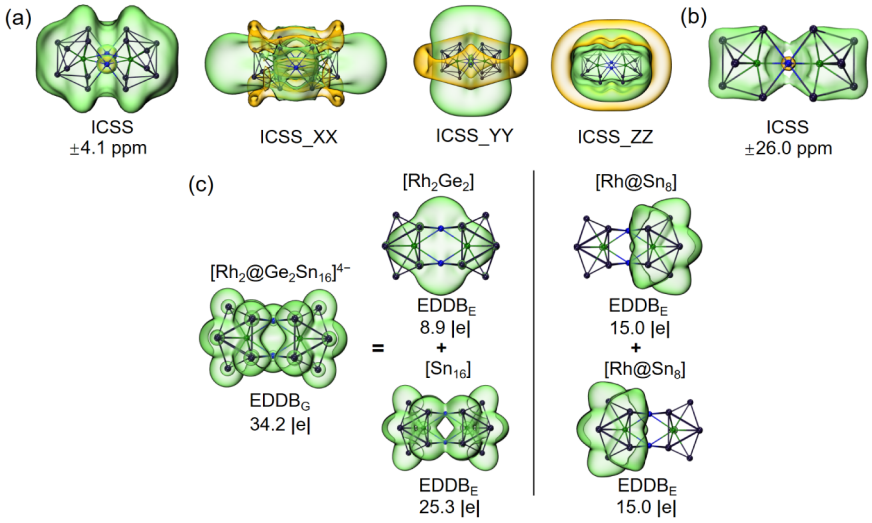

Figure 3. Calculated iso-chemical shielding surfaces (ICSSs) of cluster **1a** account for the average (NICS) and certain orientations of the external field (ICSS_XX, ICSS_YY, ICSS_ZZ). Yellow regions represent chemical shielding areas, whereas green areas represent chemical deshielding regions at an isosurface value of ± 4.1 ppm (a). The ICSS isosurface is given at ± 26.0 ppm (b) to locate the two spherical aromatic states at each aggregated cluster unit. Global ($EDDB_G$) and fragment ($EDDB_E$) electron density of delocalized bond isosurface for **1a**, and selected regions as well as those distributed for each [$RhSn_8$] unit (c). The isosurface value is set at 0.02 electrons.

fragment peaks with variable Ge/Sn ratios (Figures S8−S12), typical of other Ge/Sn mixed clusters, were also observed.[38] Energy-dispersive X-ray spectroscopy (EDX) analysis revealed an elemental ratio of K:Rh:Ge:Sn = 4.7:2:2:16.1 (Figure S13 and Table S2), in close agreement with the results from single-crystal X-ray diffraction. The slight deviation in the K content is likely due to surface irregularities caused by air exposure to the crystals. Similar to previously reported Ge/Sn clusters, the *exo*-bonding atoms in cluster **1a** are Ge rather than Sn.

Structurally, cluster **1a** can be described as two [$Rh@Sn_8$] units interconnected by two approximately square-planar [$GeSn_4$] fragments (Sn4−Sn5−Ge1−Sn10−Sn11 and Sn6−Sn8−Ge2−Sn14−Sn15; Figure 1a−e). The long and short axes of this cage are measured as 8.78 and 4.90 Å, respectively (Figure 1b). The Ge−Ge bond length (2.896 Å) is notably longer than those in previously reported Ge-based clusters (~2.4−2.6 Å)[42−48] and exceeds the sum of covalent radii (2.42 Å),[49,50] indicating the absence of direct Ge−Ge bonding interactions. The square-planar coordination observed in [$GeSn_4$] is rare among main-group systems (Figure 1d), although analogous coordination environments have been reported for several metal atoms such as [$PdAs_4$] in [Pd_2As_{14}]$^{4-}$,[51] [$AuSb_4$] in [Au_2Sb_{16}]$^{4-}$,[52] [$ZnGe_4$] in [Zn_6Ge_{16}]$^{4-}$, and [$CdGe_4$] in [Cd_6Ge_{16}]$^{4-}$.[42] Within the [$GeSn_4$] planes, the Sn−Sn bond distances are markedly elongated (Sn4−Sn11, Sn5−Sn10, Sn6−Sn14, Sn8−Sn15 = 3.384 Å; Sn4−Sn5, Sn6−Sn8 = 4.582 Å; Sn10−Sn11, Sn14−Sn15 = 4.598 Å) relative to those in conventional Sn-based clusters (~2.9−3.1 Å).[53−57] The Ge−Sn bond distances in the [$GeSn_4$] units (2.851−2.853 Å) are also longer than those observed in [$(Ge_9)Sn(Ge_9)$]$^{4-}$ (2.630−2.709 Å),[58] [$(Sn_6Ge_2Bi)_2$]$^{4-}$ (2.670−2.801 Å),[39] and the sum of covalent radii (2.61 Å),[49,50] indicating the presence of a delocalized bonding framework across the [$GeSn_4$] units. In addition, the spatial arrangement of the two Ge atoms and the two encapsulated Rh atoms creates a distinct rhombic [Rh_2Ge_2] plane (Figure 1e). The Rh−Ge distances (2.548 and 2.562 Å) fall within the range reported for Rh/Ge clusters, such as $Rh_8(CO)_{12}(\mu_4\text{-}GePh)_6$ (2.330 Å−2.698 Å)[59] and [$Rh_{23}Ge_3(CO)_{41}$]$^{5-}$ (2.506−2.818 Å).[60] The Rh−Sn distances (2.730−2.841 Å) are likewise comparable to those observed in [$Rh_2@Sn_{17}$]$^{6-}$ (2.696−2.761 Å)[56] and [$Rh_3@Sn_{24}$]$^{5-}$ (2.657−3.059 Å).[56]

To gain further insight into the electronic structure and bonding, theoretical analysis was carried out. Cluster **1a** contains a total of 94 valence electrons (2 × Ge + 16 × Sn + 2 × Rh + 4 = 2 × 4 + 16 × 4 + 2 × 9 + 4 = 94). To clearly describe the distribution of these electrons, we employed the Adaptive Natural Density Partitioning (AdNDP) analysis (Figure 2).[61] AdNDP results revealed 26 lone pairs (LPs)—five d-type LPs on each Rh atom and 16 s-type LPs on the peripheral Sn atoms—consistent with charge distribution analysis (Table S3). The outer structural framework is stabilized by eight 3c-2e Sn−Sn−Sn bonds and four 4c−2e Ge−Sn−Sn−Sn delocalized σ bonds. In addition, each [$GeSn_4$] unit features three delocalized σ bonds, consisting of one fully delocalized 5c−2e σ bond and two partially delocalized 5c−2e σ bonds. Together, these three σ bonds form a σ-sextet that obeys the (4n + 2) Hückel's rule, thereby conferring σ-aromaticity. The six remaining electrons are distributed over two 9c−2e bonds and one extensively delocalized 20c−2e bond, reinforcing the global aromaticity of the cluster. These multicenter delocalized bonding interactions illustrate extensive electron sharing between the two [$Rh@Sn_8$] subunits, establishing a net intercluster bonding connection composed of two fully delocalized 5c−2e σ bonds and the highly delocalized 20c−2e bond. Together, they account for six shared electrons between the individual cluster units, corresponding to a formal intercluster bond order of 3 and collectively define a globally aromatic, triply bonded dimeric framework.

The calculated NICS values corroborate the bonding analysis, revealing pronounced aromaticity in cluster **1a**. At 1 Å above the $GeSn_4$ fragment and at the geometric center of the cluster, the $NICS(1)_{zz}$ and NICS values are −52.56 and −17.89 ppm, respectively. The overall aromaticity of the clusters is further supported by the iso-chemical shielding surfaces (ICSS, Figure 3a,b), also known as NICS isosurfaces,

https://doi.org/10.1021/jacs.5c18030
J. Am. Chem. Soc. 2025, 147, 45723−45730

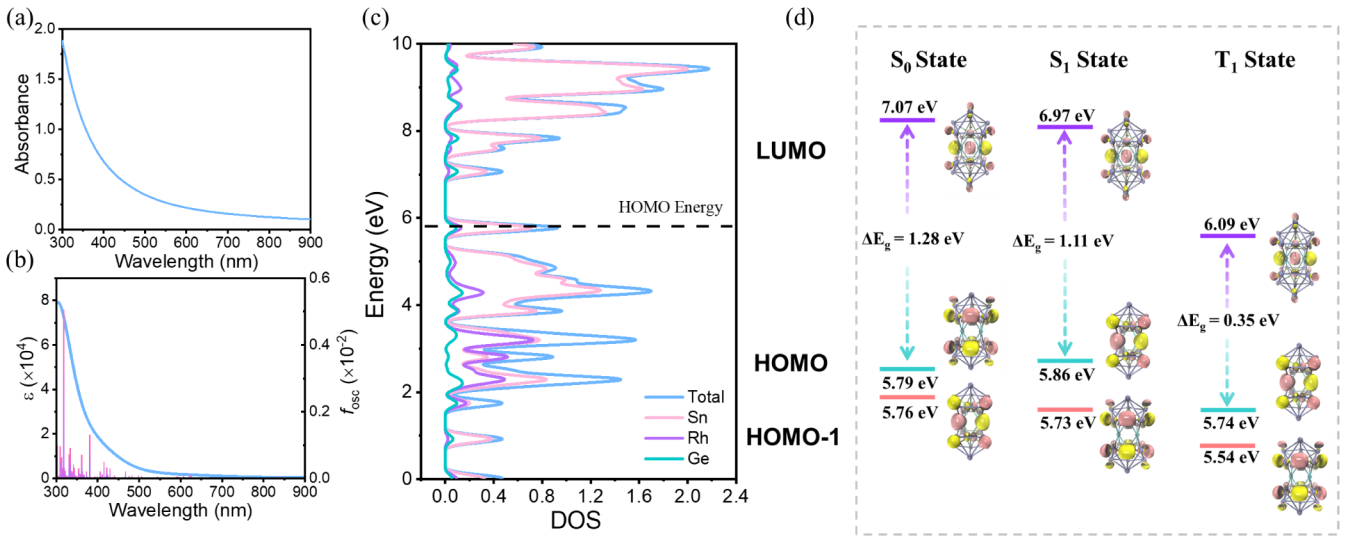

Figure 4. (a) Steady-state UV−vis absorption spectrum of $[(Rh@Sn_8)_2Ge_2]^{4-}$ in a DMF solution. (b) TD-DFT simulated UV−vis absorption spectrum of $[(Rh@Sn_8)_2Ge_2]^{4-}$ at the PBE0/def2-TZVP level. (c) Total density of states and partial density of states for $[(Rh@Sn_8)_2Ge_2]^{4-}$. Eigenvalues are broadened with a Gaussian line shape with a full width at half-maximum of 0.1 eV. (d) Frontier molecular orbital (MO) diagrams of the minimal-energy geometry for $[(Rh@Sn_8)_2Ge_2]^{4-}$ in the S_0, S_1, and T_1 states.

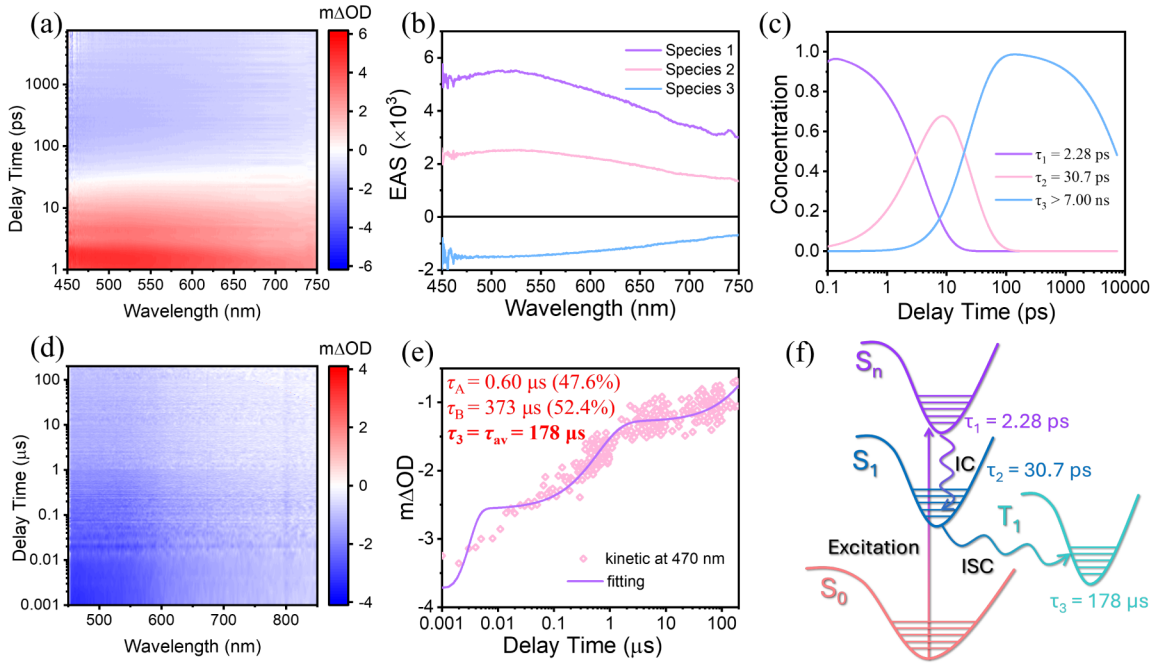

Figure 5. (a) Fs-TA contour plot, (b) EAS features obtained from the global analysis based on the sequential mode, and (c) time evolution of the state population of $[(Rh@Sn_8)_2Ge_2]^{4-}$ solution of DMF with 400 nm excitation. (d) Ns-TA contour plot and (e) single-wavelength kinetic fitting at 470 nm for $[(Rh@Sn_8)_2Ge_2]^{4-}$ solution of DMF with 400 nm excitation. (f) Schematic illustration of the photophysical mechanism of $[(Rh@Sn_8)_2Ge_2]^{4-}$ in DMF solution with 400 nm excitation.

which visualize the spatial distribution of magnetic shielding based on the calculated **XX, YY, and ZZ** tensor components.

The ICSS isosurfaces reveal a continuous shielding region involving the entire cluster structure, confirming the delocalized aromatic character of cluster **1a** (Figure 3a,b). When the external magnetic field is applied along the *x*-axis (ICSS_XX), a central shielding region accompanied by a perpendicular deshielding contour emerges, owing to the formation of a shielding cone.[62−64] Similar behavior is observed when the field is oriented along the *y*-axis, denoting that this response is an intrinsic characteristic of spherical aromatic systems.[65] Interestingly, under a *z*-axis oriented field that passes through both $[Rh@Sn_8]$ subunits, the induced shielding cones from each unit overlap directly, reminiscent of the behavior observed in previously reported linear cluster aggregates.[10,11] At an ICSS isosurface value of ± 26.0 ppm, two distinct spherical shielding domains are clearly visible, each centered on a $[Rh@Sn_8]$ unit (Figure 3b). This observation confirms that both subunits maintain an individual spherical aromaticity within the overall framework.

The electron density of delocalized bonds (EDDB) analysis further substantiates this conclusion. EDDB was evaluated for

https://doi.org/10.1021/jacs.5c18030
J. Am. Chem. Soc. 2025, 147, 45723−45730

the global cluster ($EDDB_G$) and for selected fragments ($EDDB_E$), providing the distribution and quantification of the delocalized electrons (Figure 3c).[66−68] The isosurface for $EDDB_G$ exhibits extensive delocalization across the entire cluster, corresponding to 34.2 |e| in total, partitioned into 8.9 |e| for the central $[Rh_2Ge_2]$ unit and 25.3 |e| for the remaining $[Sn_{16}]$ cage, supporting the aromatic character evaluated from AdNDP and ICSS approaches. The dissection of the delocalized electrons into each $[RhSn_8]$ unit results in 15.0 |e|, indicating that the overall aromaticity of **1a** arises from the cooperative interaction of two spherically aromatic subunits acting in concert as a single delocalized entity.

The electronic structure of the $[K(2.2.2-crypt)]_4[(Rh@Sn_8)_2Ge_2]$ nanocluster was first studied by UV−vis absorption spectroscopy in DMF solution (Figure 4a). The spectrum exhibited a broad, gradually decreasing absorption band from 300 to 900 nm, consistent with the features of the TD-DFT simulated spectrum of the $[(Rh@Sn_8)_2Ge_2]^{4-}$ anion (Figure 4b), whereas that of the $[K(2.2.2-crypt)]^+$ cation exhibited mainly absorption under 250 nm (Figure S14). Hence, the absorption feature of the $[K(2.2.2-crypt)]_4[(Rh@Sn_8)_2Ge_2]$ nanocluster is predominately contributed by the anion part. The density of states (DOS) analysis (Figure 4c) further revealed that Sn atoms contribute predominantly to the molecular orbital of the $[(Rh@Sn_8)_2Ge_2]^{4-}$ nanocluster. Furthermore, frontier molecular orbital (MO) analysis (Figure 4d) showed that, in the ground-state minimum, the highest occupied molecular orbital (HOMO) is mainly localized on the Sn atoms, whereas in the lowest unoccupied molecular orbital (LUMO), the electron cloud moves to the center Ge atoms, indicating an intracluster Sn → Ge charge-transfer (CT) character upon excitation.

The minimal-energy geometries of $[(Rh@Sn_8)_2Ge_2]^{4-}$ in its lowest singlet and triplet excited states were also optimized for comparison. As shown in Figure S15, both excited states of the nanocluster showed minimal structural distortion relative to the ground state, with most bond lengths exhibiting a slight elongation (Table S4), accounting for the structural rigidity of the overall cluster upon excitation, which in turn favors to avoid nonradiative decays. The main orbital transitions for $S_1 \rightarrow S_0$ and $T_1 \rightarrow S_0$ transitions mainly correspond to LUMO → HOMO-1 and LUMO → HOMO for the S_1 state geometry and T_1 state geometry, respectively (Tables S6 and S7), confirming the CT characteristic of both excited state species.

The excited-state behaviors of $[(Rh@Sn_8)_2Ge_2]^{4-}$ were further investigated using TA spectroscopy with 400 nm excitation, and steady-state UV−vis absorption confirmed that the feature did not change after the TA measurements (Figure S16). In the femtosecond-TA (fs-TA) spectra measured in DMF solution (Figure 5a), a broad excited-state absorption (ESA) band spanning 450−750 nm emerged immediately and then gradually decayed within 10 ps, accompanied by the generation of a broad negative ground state bleaching (GSB) signal centered at around 400 nm, which persisted beyond 7 ns (Figure 5a). Global kinetic analysis in a sequential model resolved three evolution-associated spectra (EAS) species with kinetic traces of corresponding time constants at τ_1 = 1.77 ps, τ_2 = 28.1 ps, and τ_3 > 7.00 ns, respectively (Figure 5b,c, Table S8). The first process (τ_1) can be attributed to an internal conversion (IC) process among higher singlet excited states ($S_n \rightarrow S_1$), consistent with the wavelength-dependent relaxation trend results showing the corresponding time constant would be shorter with the longer excitation wavelength (Figure S17 and Table S8). Subsequently, the lowest singlet excited state undergoes intersystem crossing (ISC) to the triplet state (τ_2). The triplet-state dynamics were further studied by nanosecond-TA (ns-TA) spectroscopy, which revealed that the GSB broad band signal consisted of two componential decay with different lifetimes of τ_A = 602 ns and τ_B = 373 μs (Figure 5d,e). The dual componential decay likely arises from the intercluster atom exchange of the nanocluster in solution (Figure S4).[69−73] Hence, the weighted average lifetime (τ_{av}, equation in Table 1) was used to evaluate

Table 1. Comparison of the Triplet State Lifetimes of the Traditional Ligand-Protected Nanoclusters and $[(Rh@Sn_8)_2Ge_2]^{4-}$

Name	Method[a]	Triplet Lifetime	ref.
Au_{44}a	TCSPC	8.97 μs[b]	74
Cu_{26}	TCSPC	6.94 μs[b]	75
Cu_{40}-H	TCSPC	8.80 μs	76
Au_2Cu_2DPA	ns-TAS	146 μs	77
Ag_xAu_{25-x}	TCSPC	9.52 μs	78
$Au_{52}(SR)_{32}$	ns-TAS	0.56 μs	79
$Au_{16}Cu_6$	ns-TAS	1.30 μs	80
Au_{22}	ns-TAS	0.60 μs	80
Au_5Ag_{11}	MCS	4.28 μs[b]	81
Pt_1Ag_{16}	MCS	2.76 μs[b]	82
$Au_{42}(SR)_{32}$	TCSPC	2.38 μs	82
Ag_{29}+Ag	ns-TAS	5.92 μs[b]	83
Au_6Ag_2	TCSPC	2.59 μs[b]	84
Au_6Ag_4	TCSPC	1.85 μs[b]	84
$[(Rh@Sn_8)_2Ge_2]^{4-}$	ns-TAS	178 μs[b]	**This work**

[a]TCSPC: time-correlated single photon counting, ns-TAS: nanosecond transient absorption spectroscopy, and MSC: multichannel scaling. [b]Weighted average lifetime:$\tau_{av} = \frac{\sum_{i=1}^{n} \tau_i A_i}{\sum_{i=1}^{n} A_i}$.

the triplet excited state of $[(Rh@Sn_8)_2Ge_2]^{4-}$, and the lifetime was determined to be $\tau_3 = \tau_{av}$ = 178 μs using the A_1 and A_2 values in Table S9. Thus, the overall photophysical mechanism of $[(Rh@Sn_8)_2Ge_2]^{4-}$ in DMF can be illustrated as Figure 5f. Notably, the lifetime of the triplet state for $[(Rh@Sn_8)_2Ge_2]^{4-}$ is significantly longer (Table 1) compared with those of traditional ligand-protected metal nanoclusters.[74−84] This exceptionally long lifetime suggested efficient excited-state stabilization within the heteroatomic core.

The lifetime of the triplet state is highly related to the energy splitting between the triplet state and the ground state, and the spin−orbit coupling (SOC) effect when the nonradiative transition is dominant based on the following equation:[85−87]

$$k_{ISC} = \frac{2\pi}{\hbar}\langle T_1|\hat{H}_{SO}|S_0\rangle^2 \frac{1}{\sqrt{4\pi k_B T}} \exp\left(-\frac{\Delta E_{TS}^2}{4\lambda k_B T}\right)$$

where $\langle T_1|\hat{H}_{SO}|S_0\rangle$ is the spin−orbit coupling matrix element (SOCME), ΔE_{TS} is the energy gap between the T_1 state and ground state, and λ is the reorganization energy. TD-DFT calculations revealed that $[(Rh@Sn_8)_2Ge_2]^{4-}$ possesses a small spin−orbit coupling matrix element (SOCME) of 0.05 cm^{-1} between T_1 and S_0 states (Figure S18), notably smaller than those of conventional metal nanoclusters exhibiting ligand-to-metal charge transfer (LMCT) or metal-to-ligand charge transfer (MLCT) excited-state features.[88] The extremely weak SOC effect facilitates slow intersystem relaxation, accounting

https://doi.org/10.1021/jacs.5c18030
J. Am. Chem. Soc. 2025, 147, 45723−45730

for the remarkably long-lived triplet state observed experimentally.

CONCLUSIONS

In summary, we have isolated and characterized a novel all-metal cluster, $[(Rh@Sn_8)_2Ge_2]^{4-}$, which expands the structural diversity of multiple-bonded intercluster aggregates, featuring spherical aromatic units connected via the unprecedented square-planar coordinated 6σ-aromatic [$GeSn_4$] bridge. The reported cluster can be interpreted as an integration of spherical aromaticity, augmented by contributions from local aromatic fragments. The discovery of an aromatic bridging unit introduces a new design principle for cluster growth through aromatic linkage, offering an alternative to conventional metal−metal bonding in the construction of extended cluster architectures. This framework provides a conceptual foundation for assembling cluster-based materials from discrete aromatic modules, thereby opening a rational path toward the hierarchical construction of bulk materials from molecular clusters. Moreover, femtosecond-nanosecond transient absorption spectroscopy revealed that $[(Rh@Sn_8)_2Ge_2]^{4-}$ possesses a remarkably long-lived triplet state (τ_{av} = 178 μs in DMF)—significantly longer than those reported for metal nanoclusters in the condensed phase. This finding fills a critical gap in the excited-state landscape of inorganic clusters and highlights σ-aromaticity as a powerful strategy for suppressing nonradiative decay and stabilizing excited states. The combined structural innovation and photophysical longevity of this system establish a new blueprint for designing functionally robust nanoclusters for photonic, catalytic, and energy-related applications.

ASSOCIATED CONTENT

Supporting Information

The Supporting Information is available free of charge at https://pubs.acs.org/doi/10.1021/jacs.5c18030.

Detailed experimental procedures, crystallographic supplementation, electrospray-ionization mass spectrometry (ESI-MS), energy-dispersive X-ray (EDX) spectroscopic analysis, transient absorption spectroscopy data, and quantum-chemical studies (PDF)

Accession Codes

Deposition Number 2484962 contains the supplementary crystallographic data for this paper. These data can be obtained free of charge via the joint Cambridge Crystallographic Data Centre (CCDC) and Fachinformationszentrum Karlsruhe Access Structures service.

AUTHOR INFORMATION

Corresponding Authors

Zhong-Ming Sun − *State Key Laboratory of Elemento-Organic Chemistry, College of Chemistry, Tianjin Key Lab for Rare Earth Materials and Applications, School of Materials Science and Engineering, Nankai University, Tianjin 300350, China*; orcid.org/0000-0003-2894-6327; Email: sunlab@nankai.edu.cn

Teng-Teng Chen − *Department of Chemistry, The Hong Kong University of Science and Technology, Hong Kong, China*; Email: tengtengchen@ust.hk

Authors

Ya-Shan Huang − *State Key Laboratory of Elemento-Organic Chemistry, College of Chemistry, Tianjin Key Lab for Rare Earth Materials and Applications, School of Materials Science and Engineering, Nankai University, Tianjin 300350, China*

Ziqi Deng − *Department of Chemistry, The Hong Kong University of Science and Technology, Hong Kong, China*

Wen-Juan Tian − *Institute of Molecular Science, Shanxi University, Taiyuan 030006, China*; orcid.org/0000-0002-1715-9216

Hui-Qing Sun − *Institute of Molecular Science, Shanxi University, Taiyuan 030006, China*

Alvaro Muñoz-Castro − *Facultad de Ingeniería, Universidad San Sebastián, Santiago 8420524, Chile*; orcid.org/0000-0001-5949-9449

Complete contact information is available at: https://pubs.acs.org/10.1021/jacs.5c18030

Author Contributions

⊥Y.-S.H. and Z.D. contributed equally to this work.

Notes

The authors declare no competing financial interest.

ACKNOWLEDGMENTS

This work was supported by the National Natural Science Foundation of China (nos. 22425107, 92461303, and 22371140 to Z.-M. Sun). W.-J. T. acknowledges the financial support from the National Natural Science Foundation of China (22402108). A.M.-C. thanks FONDECYT ANID Regular 1221676. T.-T. Chen acknowledges the start-up fund (R9874) from HKUST, the Early Career Scheme (26311224) and General Research Fund (16312125) from the Research Grants Council of Hong Kong, the Young Elite Scientists Sponsorship Program by the China Association for Science and Technology (CAST) (2023QNRC001), and open research fund of the Key Laboratory of Precision and Intelligent Chemistry.

REFERENCES

(1) Zhao, J.; Du, Q.; Zhou, S.; Kumar, V. Endohedrally doped cage clusters. *Chem. Rev.* **2020**, *120*, 9021−9163.

(2) Castleman, A. W.; Khanna, S. N. Clusters, superatoms, and building blocks of new material. *J. Phys. Chem. C* **2009**, *113* (7), 2664−2675.

(3) Doud, E. A.; Voevodin, A.; Hochuli, T. J.; Champsaur, A. M.; Nuckolls, C.; Roy, X. Superatoms in materials science. *Nat. Rev. Mater.* **2020**, *5*, 371−387.

(4) Khanna, S. N.; Jena, P. Assembling crystals from clusters. *Phys. Rev. Lett.* **1992**, *69*, 1664−1667.

(5) Cui, L. F.; Huang, X.; Wang, L. M.; Zubarev, D. Y.; Boldyrev, A. I.; Li, J.; Wang, L. S. Sn_{12}^{2-}: Stannaspherene. *J. Am. Chem. Soc.* **2006**, *128*, 8390−8391.

(6) Cui, L. F.; Huang, X.; Wang, L. M.; Li, J.; Wang, L. S. Endohedral Stannaspherenes $M@Sn_{12}^{-}$: A Rich Class of Stable Molecular Cage Clusters. *Angew. Chem., Int. Ed.* **2007**, *46*, 742−745.

(7) Goicoechea, J. M.; Sevov, S. C. $[(Pd@Pd)@Ge_{18}]^{4-}$: a palladium dimer inside the largest single-cage deltahedron. *J. Am. Chem. Soc.* **2005**, *127*, 7676−7677.

(8) Sun, Z. M.; Xiao, H.; Li, J.; Wang, L. S. $Pd_2@Sn_{18}^{4-}$: fusion of two endohedral stannaspherenes. *J. Am. Chem. Soc.* **2007**, *129*, 9560−9561.

(9) Rodríguez-Kessler, P. L.; Muñoz-Castro, A. Ligand-free supermolecules: $[Pd_2@Ge_{18}]^{4-}$ and $Pd_2@Sn_{18}]^{4-}$ as multiple-bonded zintl-ion clusters based on $Pd@Ge_9$ and $Pd@Sn_9$ assembled units. *Nanoscale* **2024**, *16*, 5829−5835.

(10) Xu, H. -L.; Tkachenko, N. V.; Szczepanik, D. W.; Popov, I. A.; Muñoz-Castro, A.; Boldyrev, A. I.; Sun, Z. -M. Symmetry collapse due

to the presence of multiple local aromaticity in Ge_{24}^{4-}. *Nat. Commun.* **2022**, *13*, 2149.
(11) Tkachenko, N. V.; Chen, W. X.; Morgan, H. W.; Muñoz-Castro, A.; Boldyrev, A. I.; Sun, Z. M. Sn_{36}^{8-}: a 2.7 nm naked aromatic tin rod. *Chem. Commun.* **2022**, *58*, 6223−6226.
(12) Kekulé, A. Sur la constitution des substances aromatiques. *Bull. Soc. Chim.* **1865**, *3*, 98−110.
(13) Faraday, M. On new compounds of carbon and hydrogen and on certain other products obtained during the decomposition of oil by heat. *Philos. Trans. R. Soc.* **1825**, *115*, 440−446.
(14) Fernández, I.; Frenking, G.; Merino, G. Aromaticity of metallabenzenes and related compounds. *Chem. Soc. Rev.* **2015**, *44*, 6452−6463.
(15) Lee, V.; Sekiguchi, A. Aromaticity of group 14 organometallics: experimental aspects. *Angew. Chem., Int. Ed.* **2007**, *46*, 6596−6620.
(16) Ota, K.; Kinjo, R. Inorganic Benzene Valence Isomers. *Chem. Asian J.* **2020**, *15*, 2558−2574.
(17) Kushvaha, S. K.; Roesky, H. W. Amidinato silylene-based inorganic aromatic rings. *Dalton Trans.* **2024**, *53*, 19058−19074.
(18) Ota, K.; Kinjo, R. Heavier element-containing aromatics of [4n +2]-electron systems. *Chem. Soc. Rev.* **2021**, *50*, 10594−10673.
(19) Chen, P.; Li, Y.; Ma, J.; Zhu, J.; Xie, J.; Solà, M.; Zhu, C.; Zhu, Q. Neutral All-Metal σ-Aromaticity in a Rhombic Cluster. *J. Am. Chem. Soc.* **2025**, *147*, 14769−14776.
(20) Freitag, K.; Gemel, C.; Jerabek, P.; Oppel, M. I.; Seidel, R. W.; Frenking, G.; Banh, H.; Dilchert, K.; Fischer, R. A. The σ-aromatic clusters $[Zn_3]^+$ and $[Zn_2Cu]$: embryonic brass. *Angew. Chem., Int. Ed.* **2015**, *54*, 4370−4374.
(21) Kuwabara, T.; Guo, J. D.; Nagase, S.; Saito, M. Diversity of the structures in a distannene complex and its reduction to generate a six-membered Ti_2Sn_4 ring complex. *Angew. Chem., Int. Ed.* **2014**, *53*, 434−438.
(22) Popov, I. A.; Boldyrev, A. I. *The Chemical Bond: chemical Bonding Across the Periodic Table*; Frenking, G.; Shaik, S.; Wiley-VCH: Weinheim, 2014; Vol. *14*, pp. 421−444
(23) Power, P. P. The synthesis, characterization and some properties of new quasi-aromatic main group ring systems. *J. Organomet. Chem.* **1990**, *400*, 49−69.
(24) Velian, A.; Cummins, C. C. Synthesis and characterization of $P_2N_3^-$: An aromatic ion composed of phosphorus and nitrogen. *Science* **2015**, *348*, 1001−1004.
(25) Fischer, M.; Nees, S.; Kupfer, T.; Goettel, J. T.; Braunschweig, H.; Hering-Junghans, C. Isolable phospha-and arsaalumenes. *J. Am. Chem. Soc.* **2021**, *143*, 4106−4111.
(26) Sarkar, S. K.; Chaliha, R.; Siddiqui, M. M.; Banerjee, S.; Münch, A.; Herbst-Irmer, R.; Stalke, D.; Jemmis, E. D.; SRoesky, H. W. A Neutral three-membered 2π aromatic disilaborirane and the unique conversion into a four-membered BSi_2N-Ring. *Angew. Chem., Int. Ed.* **2020**, *59*, 23015−23019.
(27) Fan, J.; Yue, L.; Liu, C.; Rao, B.; Zhou, G.; Li, A.; Su, B. Isolation of fluorescent 2π-aromatic 1, 3-disiladiboretenes. *J. Am. Chem. Soc.* **2024**, *146*, 39−44.
(28) Kushvaha, S. K.; Kallenbach, P.; Rohman, S. S.; Pandey, M. K.; Hendi, Z.; Rüttger, F.; Herbst-Irmer, R.; Stalke, D.; Parameswaran, P.; Roesky, H. W. A Neutral planar four-membered Si_2B_2 2π-aromatic ring. *J. Am. Chem. Soc.* **2023**, *145*, 25523−25527.
(29) Ota, K.; Kinjo, R. A Neutral and Aromatic Boron-Rich Inorganic Benzene. *Angew. Chem., Int. Ed.* **2020**, *59*, 6572−6575.
(30) Jana, A.; Huch, V.; Repisky, M.; Berger, R. J.; Scheschkewitz, D. Dismutational and global-minimum isomers of heavier 1, 4-dimetallatetrasilabenzenes of group 14. *Angew. Chem., Int. Ed.* **2014**, *53*, 3514−3518.
(31) Yao, S.; Xiong, Y.; Szilvási, T.; Grützmacher, H.; Driess, M. From a phosphaketenyl-functionalized germylene to 1, 3-digerma-2, 4-diphosphacyclobutadiene. *Angew. Chem., Int. Ed.* **2016**, *55* (55), 4781−4785.
(32) Inoue, S.; Wang, W.; Präsang, C.; Asay, M.; Irran, E.; Driess, M. An ylide-like phosphasilene and striking formation of a 4π-electron, resonance-stabilized 2, 4-disila-1, 3-diphosphacyclobutadiene. *J. Am. Chem. Soc.* **2011**, *133*, 2868−2871.
(33) Koop, A.; Gantefoer, G.; Kim, Y. Long-lived excited states in metal clusters *Phys. Chem. Chem. Phys.* **2017**, *19*, 21335.
(34) Frisch, M. J.; Trucks, G. W.; Schlegel, H. B.; Scuseria, G. E.; Robb, M. A.; Cheeseman, J. R.; Scalmani, G.; Barone, V.; Petersson, G. A.; Nakatsuji, H., et al. *Gaussian 16, Revision B.01*; Gaussian, Inc.: Wallingford, CT, 2016.
(35) Lu, T.; Chen, F. Multiwfn: A multifunctional wavefunction analyzer. *J. Comput. Chem.* **2012**, *33*, 580−592.
(36) Humphrey, W.; Dalke, A.; Schulten, K. V. Visual molecular dynamics. *J. Mol. Graph.* **1996**, *14*, 33−38.
(37) Neese, F. The ORCA program system. *WIREs Comput. Mol. Sci.* **2012**, *2*, 73−78.
(38) Gillett-Kunnath, M. M.; Petrov, I.; Sevov, S. C. Heteroatomic deltahedral Zintl ions of group 14 and their alkenylation. *Inorg. Chem.* **2010**, *49*, 721−729.
(39) Gillett-Kunnath, M. M.; Muñoz-Castro, A.; Sevov, S. C. Trimetallic deltahedral Zintl ions: experimental and theoretical studies of the novel dimer $[(Sn_6Ge_2Bi)_2]^{4-}$. *Chem. Commun.* **2012**, *48*, 3524−3526.
(40) Gillett-Kunnath, M. M.; Paik, J. I.; Jensen, S. M.; Taylor, J. D.; Sevov, S. C. Metal-centered deltahedral zintl ions: Synthesis of $[Ni@Sn_9]^{4-}$ by direct extraction from intermetallic precursors and of the vertex-fused dimer $[\{Ni@Sn_8(\mu\text{-}Ge)_{1/2}\}_2]^{4-}$. *Inorg. Chem.* **2011**, *50*, 11695−11701.
(41) Huang, Y. S.; Xu, H. L.; Tian, W. J.; Li, Z. S.; Escayola, S.; Solà, M.; Muñoz-Castro, A.; Sun, Z. M. $[Co_3@Ge_6Sn_{18}]^{5-}$: a giant σ-aromatic cluster analogous to H_3^+ and Li_3^+. *J. Am. Chem. Soc.* **2025**, *147*, 9407−9414.
(42) Xu, H. L.; Popov, I. A.; Tkachenko, N. V.; Wang, Z. C.; Muñoz-Castro, A.; Boldyrev, A. I.; Sun, Z. M. σ-aromaticity-induced stabilization of heterometallic supertetrahedral clusters $[Zn_6Ge_{16}]^{4-}$ and $[Cd_6Ge_{16}]^{4-}$. *Angew. Chem., Int. Ed.* **2020**, *59*, 17286−17290.
(43) Spiekermann, A.; Hoffmann, S. D.; Fässler, T. F.; Krossing, I.; Preiss, U. $[Au_3Ge_{45}]^{9-}$—A binary anion containing a $\{Ge_{45}\}$ cluster. *Angew. Chem., Int. Ed.* **2007**, *46*, 5310−5313.
(44) Zhou, B.; Denning, M. S.; Kays, D. L.; Goicoechea, J. M. Synthesis and isolation of $[Fe@Ge_{10}]^{3-}$: a pentagonal prismatic Zintl ion cage encapsulating an interstitial iron atom. *J. Am. Chem. Soc.* **2009**, *131*, 2802−2803.
(45) Preiing, L.; Schrenk, C.; Schnepf, A. $\{Ge_8[Fe(CO)_4]_8\}^{7-}$: an anionic cubic germanium-iron-cluster featuring an unpaired electron. *Dalton Trans.* **2022**, *51*, 8177−8181.
(46) Schenk, C.; Schnepf, A. $Ge_{14}[Ge(SiMe_3)_3]_5Li_3(THF)_6$: the largest metalloid cluster compound of germanium: on the way to fullerene-like compounds? *Chem. Commun.* **2008**, *38*, 4643−4645.
(47) Ugrinov, A.; Sevov, S. C. Derivatization of deltahedral Zintl ions by nucleophilic addition: $[Ph{-}Ge_9{-}SbPh_2]^{2-}$ and $[Ph_2Sb{-}Ge_9{-}Ge_9{-}SbPh_2]^{4-}$. *J. Am. Chem. Soc.* **2003**, *125*, 14059−14064.
(48) Xu, H. L.; Qiao, L.; Sun, Z. M. Orientational Isomerism and Its Reactivity of a Main Group Sandwich Anion $[Ge_9\text{-}In\text{-}Ge_9]^{5-}$. *Chin. J. Chem.* **2023**, *41*, 2432−2438.
(49) Pauling, L. Atomic radii and interatomic distances in metals. *J. Am. Chem. Soc.* **1947**, *69*, 542−553.
(50) Pyykkö, P.; Atsumi, M. Molecular single-bond covalent radii for elements 1−118. *Chem.—Eur. J.* **2009**, *15*, 186−197.
(51) Reber, A. C.; Mandal, S.; Qian, M.; Saavedra, H. M.; Weiss, P. S.; Khanna, S. N.; Sen, A. Palladium in the gap: cluster assemblies with band edges localized on linkers. *J. Phys. Chem. C* **2012**, *116*, 10207−10214.
(52) Popov, I. A.; Pan, F. X.; You, X. R.; Li, L. J.; Matito, E.; Liu, C.; Zhai, H. J.; Sun, Z. M.; Boldyrev, A. I. Peculiar all-metal σ-aromaticity of the $[Au_2Sb_{16}]^{4-}$ anion in the solid state. *Angew. Chem., Int. Ed.* **2016**, *55*, 15344−15346.
(53) Wilson, R. J.; Lichtenberger, N.; Weinert, B.; Dehnen, S. Intermetalloid and heterometallic clusters combining p-block (semi) metals with d-or f-block metals. *Chem. Rev.* **2019**, *119*, 8506−8554.

https://doi.org/10.1021/jacs.5c18030
J. Am. Chem. Soc. 2025, 147, 45723−45730

(54) Kesanli, B.; Halsig, J. E.; Zavalij, P.; Fettinger, J. C.; Lam, Y. F.; Eichhorn, B. W. Cluster growth and fragmentation in the highly fluxional platinum derivatives of Sn_9^{4-}: Synthesis, characterization, and solution dynamics of $Pt_2@Sn_{17}^{4-}$ and $Pt@Sn_9H_3$. *J. Am. Chem. Soc.* **2007**, *129*, 4567−4574.
(55) Esenturk, E. N.; Fettinger, J. C.; Eichhorn, B. W. Synthesis, structure, and dynamic properties of $[Ni_2Sn_{17}]^{4-}$. *J. Am. Chem. Soc.* **2006**, *128*, 12−13.
(56) Liu, C.; Jin, X.; Li, L. J.; Xu, J.; McGrady, J. E.; Sun, Z. M. Synthesis and structure of a family of rhodium polystannide clusters $[Rh@Sn_{10}]^{3-}$, $[Rh@Sn_{12}]^{3-}$, $[Rh_2@Sn_{17}]^{6-}$ and the first triply-fused stannide, $[Rh_3@Sn_{24}]^{5-}$. *Chem. Sci.* **2019**, *10*, 4394−4401.
(57) Yang, Y. N.; Qiao, L.; Sun, Z. M. $[Cd(Sn_9)_2]^{6-}$ and $[Cd(Ni@Sn_9)_2]^{6-}$: Reactivity and coordination chemistry of empty and Ni-centered $[Sn_9]^{4-}$ Zintl ions. *Chin. Chem. Lett.* **2023**, *34*, 107207.
(58) Bentlohner, M. M.; Jantke, L. -A.; Henneberger, T.; Fischer, C.; Mayer, K.; Klein, W.; Fässler, T. F. On the nature of bridging metal atoms in intermetalloid clusters: synthesis and structure of the metal-atom-bridged Zintl clusters $[Sn(Ge_9)_2]^{4-}$ and $[Zn(Ge_9)_2)]^{6-}$. *Chem.—Eur. J.* **2016**, *22*, 13946−13952.
(59) Adams, R. D.; Smith, J. L. Rhodium cluster complexes containing bridging phenylgermanium ligands. *Inorg. Chem.* **2005**, *44*, 4276−4281.
(60) Femoni, C.; Iapalucci, M. C.; Ruggieri, S.; Zacchini, S. From mononuclear complexes to molecular nanoparticles: the buildup of atomically precise heterometallic rhodium carbonyl nanoclusters. *Acc. Chem. Res.* **2018**, *51*, 2748−2755.
(61) Zubarev, D. Y.; Boldyrev, A. I. Developing paradigms of chemical bonding: adaptive natural density partitioning. *Phys. Chem. Chem. Phys.* **2008**, *10*, 5207−5217.
(62) von Schleyer, P. R.; Jiao, H. What is aromaticity? *Pure Appl. Chem.* **1996**, *68*, 209−218.
(63) Merino, G.; Heine, T.; Seifert, G. The induced magnetic field in cyclic molecules. *Chem.—Eur. J.* **2004**, *10*, 4367−4371.
(64) Islas, R.; Heine, T.; Merino, G. The induced magnetic field. *Acc. Chem. Res.* **2012**, *45*, 215−228.
(65) Tkachenko, N. V.; Popov, I. A.; Kulichenko, M.; Fedik, N.; Sun, Z.- M.; Muñoz-Castro, A.; Boldyrev, A. I. Bridging aromatic/antiaromatic units: recent advances in aromaticity and antiaromaticity in main-Group and transition-metal clusters from bonding and magnetic analyses. *Eur. J. Inorg. Chem.* **2021**, *41*, 4239−4250.
(66) Szczepanik, D. W.; Andrzejak, M.; Dominikowska, J.; Pawełek, B.; Krygowski, T. M.; Szatylowicz, H.; Solà, M. The electron density of delocalized bonds (EDDB) applied for quantifying aromaticity. *Phys. Chem. Chem. Phys.* **2017**, *19*, 28970−28981.
(67) Szczepanik, D. W.; Żak, E.; Dyduch, K.; Mrozek, J. Electron delocalization index based on bond order orbitals. *Chem. Phys. Lett.* **2014**, *593*, 154−159.
(68) Szczepanik, D. W. *Run EDDB program*. aromaticity.uj.edu.pl/RunEDDB.R. (accessed 11 Feburary 2024).
(69) Rudolph, R.; Wilson, W.; Parker, F.; Taylor, R. C.; Young, D. Nature of naked-metal-cluster polyanions in solution. Evidence for $(Sn_{9-x}Pb_x)^{4-}$ (x = 0−9) and tin-antimony clusters. *J. Am. Chem. Soc.* **1978**, *100*, 4629−4630.
(70) Scharfe, S.; Fässler, T. F.; Stegmaier, S.; Hoffmann, S. D.; Ruhland, K. $[Cu@Sn_9]^{3-}$ and $[Cu@Pb_9]^{3-}$: intermetalloid clusters with endohedral Cu atoms in spherical environments. *Chem.− Eur. J.* **2008**, *14*, 4479−4483.
(71) Frischhut, S.; Fässler, T. F. Synthesis of low-oxidation-state germaniumclusters comprising a functional anchor group−synthesis and characterization of $[(Ge^0)_5(Ge\text{-}R)_3(Ge\text{-}(CH_2)_n\text{-}CH = CH_2)]$ with R = $Si(SiMe_3)_3$. *Dalton Trans.* **2018**, *47*, 3223−3226.
(72) Eichhorn, B. W. Zintl ions: Principles and Recent Developments. In *Book Series: structure and Bonding*, Fässler, T. F., Eds.; Springer-Verlag, Heidelberg, 2011; Vol. *140*.
(73) Corbett, J. D. Book review of zintl phases: principles and recent developments. *J. Am. Chem. Soc.* **2011**, *133*, 19562−19562.
(74) Si, W.-D.; Zhang, C.; Zhou, M.; Wang, Z.; Feng, L.; Tung, C.-H.; Sun, D. Arylgold nanoclusters: Phenyl-stabilized Au_{44} with thermal-controlled NIR single/dual-channel phosphorescence. *Sci. Adv.* **2024**, *10*, No. eadm6928.
(75) Zhang, C.; Si, W.-D.; Wang, Z.; Dinesh, A.; Gao, Z.-Y.; Tung, C.-H.; Sun, D. Solvent-mediated hetero/homo-phase crystallization of copper nanoclusters and superatomic kernel-related NIR phosphorescence. *J. Am. Chem. Soc.* **2024**, *146*, 10767−10775.
(76) Liu, L.-J.; Zhang, M.-M.; Deng, Z.; Yan, L.-L.; Lin, Y.; Phillips, D. L.; Yam, V. W.-W.; He, J. NIR-II emissive anionic copper nanoclusters with intrinsic photoredox activity in single-electron transfer. *Nat. Commun.* **2024**, *15*, 4688−4699.
(77) Arima, D.; Hidaka, S.; Yokomori, S.; Niihori, Y.; Negishi, Y.; Oyaizu, R.; Yoshinami, T.; Kobayashi, K.; Mitsui, M. Triplet-mediator ligand-protected metal nanocluster sensitizers for photon upconversion. *J. Am. Chem. Soc.* **2024**, *146*, 16630−16638.
(78) Mitsui, M.; Arima, D.; Kobayashi, Y.; Lee, E.; Niihori, Y. On the origin of photoluminescence enhancement in biicosahedral Ag_xAu_{25-x} nanoclusters (x = 0−13) and their application to triplet−triplet annihilation photon upconversion. *Adv. Optical Mater.* **2022**, *10*, 2200864.
(79) Zeng, L.; Wang, Y.; Tan, J.; Pei, Q.; Kong, J.; Zhang, W.; Ye, S.; Jin, R.; Luo, Y.; Zhou, M. Accelerated intersystem crossing enhances NIR emission in $Au_{52}(SR)_{32}$ nanoclusters by surface ligand engineering. *Chem. Sci.* **2025**, *16*, 18844−18851.
(80) Shi, W.-Q.; Zeng, L.; He, R.-L.; Han, X.-S.; Guan, Z.-J.; Zhou, M.; Wang, Q.-M. Near-unity NIR phosphorescent quantum yield from a room-temperature solvated metal nanocluster. *Science* **2024**, *383*, 326−330.
(81) Zhu, C.; Xin, J.; Li, J.; Li, H.; Kang, X.; Pei, Y.; Zhu, M. Fluorescence or phosphorescence? the metallic composition of the nanocluster kernel does matter. *Angew. Chem., Int. Ed.* **2022**, *61*, No. e202205947.
(82) Luo, L.; Liu, Z.; Du, X.; Jin, R. Near-infrared dual emission from the $Au_{42}(SR)_{32}$ nanocluster and tailoring of intersystem crossing. *J. Am. Chem. Soc.* **2022**, *144*, 19243−19247.
(83) Takano, S.; Hirai, H.; Nakashima, T.; Iwasa, T.; Taketsugu, T.; Tsukuda, T. Photoluminescence of doped superatoms $M@Au_{12}$ (M = Ru, Rh, Ir) homoleptically capped by $(Ph_2)PCH_2P(Ph_2)$: efficient room-temperature phosphorescence from $Ru@Au_{12}$. *J. Am. Chem. Soc.* **2021**, *143*, 10560−10564.
(84) Zhang, W.; Kong, J.; Liu, W.-T.; Zhao, R.; Zhang, J.; Deng, H.; Lei, Z.; Wang, Q.-M.; Luo, Y.; Zhou, M. Atomic-level engineering of Au−Ag nanoclusters enables divergent triplet emission. *Angew. Chem., Int. Ed.* **2025**, *64*, No. e202515551.
(85) Deng, Z.; Li, L.; Jia, H.; Li, N.-F.; He, J.; Li, M.-D.; Phillips, D. L.; Li, Y. Insights into the Photodynamics of Fluorescence Emission and Singlet Oxygen Generation of Fluorogen Activating Protein-Malachite Green Systems. *Chem.—Eur. J.* **2023**, *29*, No. e202203684.
(86) Deng, Z.; Huang, G.; Li, J.; Pang, J.; He, J.; Phillips, D. L.; Li, M.-D. High-level reverse intersystem crossing of charge transfer compounds: to fluoresce or not tofluoresce? *Phys. Chem. Chem. Phys.* **2024**, *26*, 17809.
(87) Deng, Z.; Huang, C.; Luo, Y.; He, J.; Li, L.; Pang, X.; Huang, G.; Phillips, D. L. Revealing the excited-state mechanisms of the polymorphs of a hot exciton material. *Nat. Commun.* **2025**, *16*, 258.
(88) Han, Z.; Duan, C.; Dong, X. Y.; Si, Y.; Hu, J. H.; Wang, Y.; Zhai, S. M.; Lu, T.; Xu, H.; Zang, S. Q.; et al. Tightly bonded excitons in chiral metal clusters for luminescent brilliance. *Nat. Commun.* **2025**, *16*, 1867.

https://doi.org/10.1021/jacs.5c18030
J. Am. Chem. Soc. 2025, 147, 45723−45730